ELSEVIER

Biophysical Chemistry

Biophysical Chemistry 83 (2000) 121–140

www.elsevier.nl/locate/bpc

Self-assembled complexes of oligopeptides and metalloporphyrins: measurements of the reorganization and electronic interaction energies for photoinduced electron-transfer reactions

Mohamed Aoudia[a], Anton B. Guliaev[b], Neocles B. Leontis[b], Michael A.J. Rodgers[b,*]

[a] *Department of Chemistry, College of Science, Sultan Qaboos University, P.O. Box 50, Al-Khod, Oman*
[b] *Center for Photochemical Sciences, Department of Chemistry, Bowling Green State University, Bowling Green, OH 43403, USA*

Received 5 August 1999; received in revised form 25 October 1999; accepted 25 October 1999

Abstract

Cationic porphyrins form ground state electrostatically associated complexes with anionic oligo-electrolytes such as those formed by a series of glutamic acid (E) residues. Temperature dependencies were measured of the rate constants for intra-complex electron transfer to the triplet state of $Pd(II)TMPyP^{4+}$ from a tyrosine (tyr, Y) or tryptophan (trp, W) moiety connected to a glutamic acid tetramer. In complexes such as YE_4, E_2YE_2, $YE_4G_{10}E$ (G, glycine), and WE_4 these data were used to estimate the reorganization energy (λ) and electronic interaction energy (H_{DA}) relevant to the process. For all tyr–peptide complexes, λ values were found to be large ($\lambda \sim 1.60 \pm 0.06$ eV), reflecting a relatively high medium polarity in the vicinity of tyr residues. It further indicates that the tyr residues in all oligo-peptides are exposed to the aqueous medium in a similar way irrespective of the position of the aromatic moiety in the peptide chain. A significantly lower λ value ($\lambda = 1.08$ eV) was derived for the tryptophan-containing peptide complex, indicating a relatively higher hydrophobic character of trp compared to tyr. The electronic coupling matrix elements (H_{DA}) derived for tyr–peptide complexes (5.1 meV for YE_4, 5.4 meV for $YE_4G_{10}E$ and 7.5 meV for E_2YE_2) were larger than that found for WE_4 (1.1 meV). Molecular dynamics calculations were employed to obtain structural features of the porphyrin–peptide complexes. These showed average distances between the center of mass (COM) of the porphyrin ring and the center of mass of the amino acid aromatic ring of 816 ± 140 pm (YE_4), 800 ± 80 pm (E_2YE_2), 900 ± 130 pm ($YE_4G_{10}E$) and 970 ± 160 pm (WE_4). The molecular dynamics calculations were shown to be in good agreement with the experimentally determined electronic interaction energies, strongly suggesting that H_{DA} is primarily responsible for the dependence of the electron-transfer rate constant (k_{ET}) on the donor–acceptor separation distance and relative orientation. The higher H_{DA} (7.55 meV) derived for tyr incor-

* Corresponding author. Tel.: +1-4193727607; fax: +1-4193729300.
E-mail address: rodgers@bgnet.bgsu.edu (M.A.J. Rodgers)

PII: S0301-4622(99)00128-3

porated into the middle of the peptide backbone (E_2YE_2) was presumed to be associated with a higher degree of orbital overlap due to a more favorable ring–ring orientation. Overlap parameters (β derived for all peptide–porphyrin complexes were similar ($\sim 0.95 \pm 0.06$ Å^{-1}), being in good agreement with most literature values for similar systems. Finally, the intra-complex electron-transfer ratio (k_{trp}/k_{tyr}) derived from flash photolysis experiments and the corresponding ratio derived from Marcus' theory combined with experimental data from the temperature-dependence investigations and electrochemical measurements were found to be in excellent agreement. This same consistency was found for the couple E_4Y and E_2YE_2. The empirical expression (Moser and Dutton) governing the intraprotein electron-transfer rate constant in native systems combined with our experimental data (k_{ET}, λ, ΔG^0) yielded tunneling pathway distances in excellent agreement with those arising from the molecular modeling studies. The exception was for the long peptide $YE_4G_{10}E$, for which the Quenched Molecular Dynamic (QMD) sampling technique was complicated and is probably inadequate.

Keywords: Photoinduced electron transfer; Reorganization energy; Electronic coupling; Oligopeptide; Metalloporphyrin

1. Introduction

In recent years, considerable research, both experimental [1–6] and theoretical [7–9], has been carried out in an effort to understand electron-transfer (ET) reactions in proteins. One result of these studies is that the kinetics of long-range electron transfer (LRET) have been shown to depend [10] on several parameters. These include the thermodynamic driving force of the reaction (ΔG^0), the electronic coupling between the electron donor and acceptor (H_{DA}), and the energy required for reorganization of the nuclear frameworks of the reactants, products, and solvent as a result of the charge shifts (λ). Among these factors, the effect of the driving force is well documented, and numerous investigations have provided evidence for a dependence of the electron-transfer rate constant (k_{ET}) on the free energy of the reaction [11–15]. Thus, in line with Marcus' predictions [7,16] the rate constant increases sharply with the driving force ($-\Delta G^0$) to a maximum at $\Delta G^0 = \lambda$ and then decreases with increasing ΔG^0 in the inverted region $-\Delta G^0 < \lambda$. The two other crucial quantities controlling the electron-transfer rate kinetics, namely, the reorganization energy (λ) and the electronic coupling element, H_{DA}, linking the local acceptor and donor sites, have been determined both experimentally [17,18] and theoretically [19–24]; and in some cases, the two approaches are in conflict [25–28]. It is clear that a major theoretical challenge still remains in developing reliable models for λ and H_{DA} that consider a detailed accounting of the electronic structure of the donor (D) and acceptor (A) partners (D/A sites, intervening matrix, etc.) as well as the dipolar response of the surrounding medium.

Models for λ based on point-charge solute species in dielectric continuum cavities were shown to be sufficient only in special cases where the donor–acceptor partners have simple shapes (e.g. spherical, bi-spherical, or ellipsoidal) [29–31]. More sophisticated models were developed in which the complex reactants are represented quantum mechanically and enclosed in dielectric cavities realistically adapted to their shape [32].

Methods for calculating H_{DA} in electron-transfer reactions have been proposed by a number of groups, and two main approaches were considered. The first approach [33–36] relies on a detailed structure of the protein; as a result, electron-transfer rates have a complex dependence on the distance r over which the ET occurs. By contrast, in the second approach [37,38] the exact structure of the protein is held to be unimportant and the parameters r, ΔG^0, and λ are sufficient to determine the ET rate constant. In this case, the ET rate dependence on the transfer distance often displays a simple exponential functional form. Evenson and Karplus [39] have proposed a detailed model showing that the conflicting pictures of these two different approaches can be reconciled.

Thus, much progress has been made in the study of electron transfer in proteins and polypeptides where the donor and acceptor groups

are joined through covalent links [40–46], and on non-covalently linked model systems [47–52].

Recent investigations in this laboratory [53] have demonstrated electron transfer originating from tyrosine (tyr, Y) or tryptophan (trp, W) moieties to a porphyrin triplet state when the porphyrin and the Y (or W) were in proximity in electrostatically associated oligopeptide–porphyrin complexes. The oligopeptides consisted of a string of four glutamic acid (glu, E) residues terminated at the N-terminus either by tryptophan (WE_4) or tyrosine (YE_4). The deprotonated side-chain carboxylic acid residues of the glutamic acids were shown to act as ion-pairing sites for a tetra-cationic palladium (II)-tetra-(*N*-methyl-4-pyridyl)porphyrin ($PdTMPyP^{4+}$). In such self-assembled ion pairs where porphyrin is not covalently linked but held in position by the peptide environment, evidence was found for an unimolecular intra-complex electron transfer from the Y and W moieties to the porphyrin triplet state [53].

In the present study, attention has been turned to the effect of the reorganization energy λ and the electron coupling (H_{DA}) matrix element linking the donor (aromatic residue) and the acceptor (porphyrin triplet state). To achieve this, the temperature dependence of the electron-transfer rate constant was used to determine the magnitude of these two quantities and their contributions to the electron-transfer rate constant. In addition to the oligopeptides YE_4 and WE_4 mentioned above, the peptides E_2YE_2 and $YE_4G_{10}E$ (G = glycine) were synthesized and studied. The E_2YE_2 system was prepared to investigate the effect of incorporating the tyrosine residue centrally within the peptide backbone, one possibility being that this positioning might affect the separation distance and relative orientation (and thence k_{ET}) between the donor and the acceptor. The longer $YE_4G_{10}E$ was prepared on the assumption that such an oligopeptide might assume a non-linear structure, which may influence the electron-transfer event. This study has been motivated by the hypothesis that these oligopeptide–porphyrin ion-pair complexes can serve as simple yet realistic models for investigating the dynamic behavior of chromoproteins.

The theory of electron-transfer reactions is now highly developed, encompassing classical, semiclassical and quantum-mechanical methods [10,54]. For non-adiabatic electron-transfer reactions, such as long-range electron transfer in proteins, the rate constant for transfer of an electron from one site to another can be formulated from the Fermi Golden Rule:

$$k_{ET} = (2\pi/\hbar)/H_{DA}^2 FC \tag{1}$$

where H_{DA} is the electronic coupling matrix element between donor and acceptor and FC is the nuclear Franck–Condon factor. This latter can be expressed quantum-mechanically [55,56], semiclassically [57], or classically [10]. Of these, the classical model of the outer-sphere electron-transfer reaction developed by Marcus [7,58], Hush [59], and Sutin [60], among others, provides a clear physical insight and has been fundamental to understanding of a wide range of processes in chemical and biochemical systems. According to this classical model, the Franck–Condon factor can be expanded according to:

$$\mathrm{FC} = (4\pi\lambda k_B T)^{-1/2} \exp\left\{ -(\Delta G^0 + \lambda)^2 / (4\lambda k_B T) \right\} \tag{2}$$

where ΔG^0 is the standard free energy of the reaction for the donor–acceptor pair, λ is the reorganization energy, k_B is the Boltzman constant, and T is the temperature. The overall expression for the electron-transfer reaction may then be written as:

$$k_{ET} = (2\pi/\hbar)\left[H_{DA}^2/(4\pi k_B \lambda T)^{1/2} \right] \exp\left\{ -(\Delta G^0 + \lambda)^2/(4\lambda k_B T) \right\} \tag{3}$$

Thus a plot of $\ln(k_{ET}T^{1/2})$ vs. $1/T$ should be linear and λ and H_{DA} can be evaluated provided ΔG^0 is known. The value of ΔG^0 for the electron-transfer reaction was calculated from the measured reduction potentials of the tyr–peptide and trp–peptide complexes [53] and the known redox potential of the triplet state of $PdTMPyP^{4+}$.

It was found that insertion of a tyrosine (or tryptophan) residue into the peptide matrix did not perturb its reduction potential [53]. However, the redox potential E^0 of the tyrosine residue in the $YE_4G_{10}E$ peptide could not be measured due to the low solubility of this peptide. For this peptide, therefore, E^0 was assumed to be similar to that in other tyr–peptides.

Analyses employing Eq. (3) need to be undertaken with care since both λ and ΔG^0 may vary with temperature [61]. In charge separation reactions, ΔG^0 decreases as the temperature is lowered [62]. In charge-shift ET reactions, Liang et al. [63] reported that λ for electron transfer across a steroid in tetrahydrofuran increased by 20% over the temperature range from 100°C to −94°C, whereas ΔG^0 was only weakly dependent on the temperature. If one assumes the temperature dependence of λ is the same for charge shifts and charge-separation reactions, then λ and ΔG^0 change in opposite directions as T is varied. Thus, temperature-dependent changes in λ may be compensated for by opposing changes in ΔG^0. However, the temperature dependencies of the λ and ΔG^0 terms appearing in the exponential term in Eq. (3) may not cancel. It is also relevant to note that for most liquid solvents λ does not vary by more than 5% over a 100°C temperature range [57]. Thus analysis based on Eq. (3) has been carried out in which the λ and ΔG^0 terms were assumed to be independent of temperature in the range employed in this study (10–60°C). In fact, this assumption will be shown to be realistic for the systems investigated here (see Section 4).

2. Experimental section

2.1. Materials and procedures

The solid phase synthesis of the different peptides and the purification and characterization were carried out using the procedures that have been fully described in the recent report from this laboratory [53]. All solutions were buffered at pH 7 [53], unless specified otherwise.

Flash photolysis experiments were performed with the second harmonic (532 nm) of a Continuum Surelite I Q-switched Nd:YAG laser that provided 6-ns pulses. Transient absorbance was monitored at right angles to the laser excitation beam using a computer-controlled kinetic spectrophotometer, which has been described elsewhere [64]. Temperature-dependent flash photolysis investigations were performed using a quartz cuvette placed in a jacketed holder supplied with water from a controlled-temperature bath. A temperature probe (Type J thermocouple, Barnant 90) was immersed in the solution out of the light path to monitor the temperature of the sample. Reduction potentials were measured by cyclic voltammetry [53].

2.2. Molecular modeling

Tetra-(*N*-methyl-4-pyridyl)porphyrin molecule ($TMPyP^{4+}$) was modeled as two fragments, one comprising the porphine nucleus and the other the 4-*N*-methyl-pyridinium pendant groups arranged symmetrically at the *meso* positions. The Spartan 4.0 program (Wavefunction, Inc.) was used for the quantum mechanical calculations of atomic point charges. Allyl groups were attached at the *meso* positions of the porphine to model the sp^2 carbon of the pendant groups. Likewise, in modeling the 4-*N*-methyl-pyridinium pendant groups, allyl groups were attached to the *para* positions to model the sp^2 hybridized *meso* carbons of the porphine. The geometries were optimized with Spartan 4.0 using ab initio methods at the 3–21G basis set level. Calculated bond distances and torsion angles compared favorably with those obtained from the crystallographically determined structure [65] of $TMPyP^{4+}$. To obtain atom-centered charges, a single-point ab initio calculation was performed at the 6–311G* level using the optimized coordinates. Atom-centered charges for the porphyrin were calculated by fitting to the electrostatic potential calculated from the electron density using routines supplied in Spartan 4.0. AMBER 5 [66] atom types were assigned according to published guidelines [67]. Torsion and bond stretching constants were calculated according to bond length [67]. AMBER 5 topology and parameter files for $TMPyP^{4+}$ and all peptides were generated using the xLeap module of AMBER 5. The peptides were subjected to 2000 steps of steepest descent minimization.

Molecular Dynamics (MD) were employed to dock the peptides to the porphyrin. Starting positions for these MD runs were generated manually by orienting the peptide at six different positions equally spaced along a 90° arc at 2–2.5 nm distance from the center of porphyrin. The starting configurations were subjected to free MD runs of 100 000 steps (1-fs increments) at 300 K using a distance-dependent dielectric function to mimic the presence of water solvent. The SHAKE option was used to constrain all bonds involving hydrogen. The last 30 ps were averaged and the average structure was minimized.

After docking a given peptide to $TMPyP^{4+}$, Quenched Molecular Dynamics (QMD) methods were used to sample the conformational space accessible for each of the four complexes, $YE_4/TMPyP^{4+}$, $WE_4/TMPyP^{4+}$, $E_2YE_2/TMPyP^{4+}$, and $YE_4G_{10}E/TMPyP^{4+}$. Every QMD run began with an energy-minimized porphyrin–peptide complex obtained by MD docking and consisted of 200 ps at high temperature (1000 K). The initial complex was heated to 1000 K during the first 20 ps of MD and was allowed to equilibrate at this temperature for an additional 30 ps. During the final 150 ps of the trajectory, structure 'snapshots' were recorded every 3 ps, thus generating 50 structures. Two separate QMD runs, each generating 50 conformations, were carried out to generate a total of 100 for each peptide–porphyrin complex. Each of the 'snapshot' conformations obtained at high temperature was energy-minimized by performing 10 ps of MD with cooling from 100 K to 0 K. The structures were subsequently equilibrated to 300 K by gradual heating over 10 ps. They were maintained at this temperature for an additional 30 ps, during which time the distance between the center of mass (COM) of the porphyrin chromophore (porphyrin ring) and the COM of the amino acid chromophore (aromatic ring system) was monitored using the CARNAL module of AMBER 5. The angle between the chromophore planes was also monitored. During the final 5 ps of each trajectory, the structures were energy-minimized by cooling to 0 K. The minimized structures were analyzed for their conformational features.

3. Results

3.1. Temperature dependence study

In an argon-saturated aqueous solution at pH 7 in the absence of peptides, the decay of the

Table 1
Experimental parameters for the intra-complex electron transfer reaction in the different oligopeptide–metalloporphyrin complexes investigated

Peptide	YE_4	YE_4	E_2YE_2	$YE_4G_{10}E$	WE_4
pH	7.0	8.2	7.0	7.0	7.0
ΔG^0 (eV)	0.25	0.32	0.25	0.25[a]	0.18
k_{ET} s^{-1} (298 K) ± 10%	6.6×10^6	9.3×10^6	1.47×10^7	4.7×10^6	1.4×10^7
H_{DA} (meV) ± 15%	5.1	5.3	7.55	5.4	1.1
λ ± 0.05 (eV)	1.57	1.65	1.56	1.61	1.08
E (meV)	278	268	275	289	187
r (pm)[b]	816 ± 140	–	800 ± 80	900 ± 130	970 ± 160
r (pm)[c]	791	–	737	794	921
β ± 0.06 $Å^{-1}$	0.95	–	0.93	0.85[d] (0.97[e])	0.96

[a] Assumed value (see text).
[b] Values determined by molecular modeling.
[c] Values derived from Eq. (8).
[d] Value estimated from Eq. (3), using r given by molecular modeling.
[e] Value estimated from Eq. (3), using r calculated from Eq. (8) (see text).

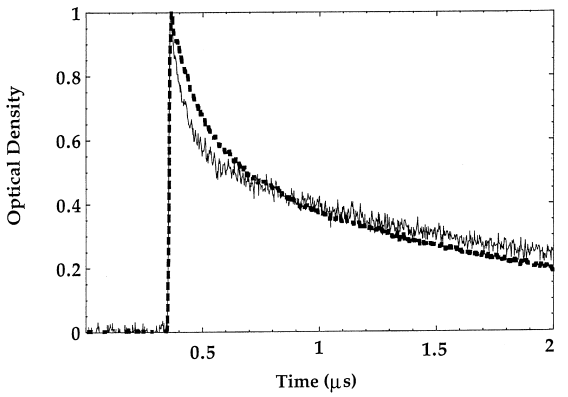

Fig. 1. Decay of the absorbance change at 460 nm following 532-nm laser excitation for an argon-saturated neutral aqueous solution of $PdTMPyP^{4+}$ (10 μM) in the presence of YE_4 (broken line) and WE_4 (solid lane) at 94 μM peptide concentration.

$PdTMPyP^{4+}$ triplet state (T_1), generated by a single 6-ns pulse of laser irradiation at 532 nm, was strictly mono-exponential with a lifetime (τ_o) of 125 μs [53]. The inclusion of the target-containing oligopeptide (20–200 μM) into the solution resulted in the porphyrin triplet state decay becoming much more rapid and bi-exponential, such that all T_1 had been removed from the system within approximately 10 μs (Fig. 1). For all peptides employed, the early decay component had a rate constant that was independent of peptide concentration, whereas the slower one was first order in peptide concentration. In the earlier publication from this laboratory, the fast process was shown to be associated with electron transfer from the target amino acid residue to the porphyrin triplet state [53]. The slower contribution to the T_1 decay arises from the fraction of the equilibrium ground state population that is not involved in complex formation prior to the excitation pulse, but which undergoes diffusive formation of an encounter complex between porphyrin and peptide molecules. This intermolecular reaction is of no further concern in what follows. Intra-complex electron-transfer rate constants were measured at room temperature for the peptide complexes and are collected in Table 1.

The temperature dependence of the intra-complex rate constant was measured for the different peptide–porphyrin complexes and the data were

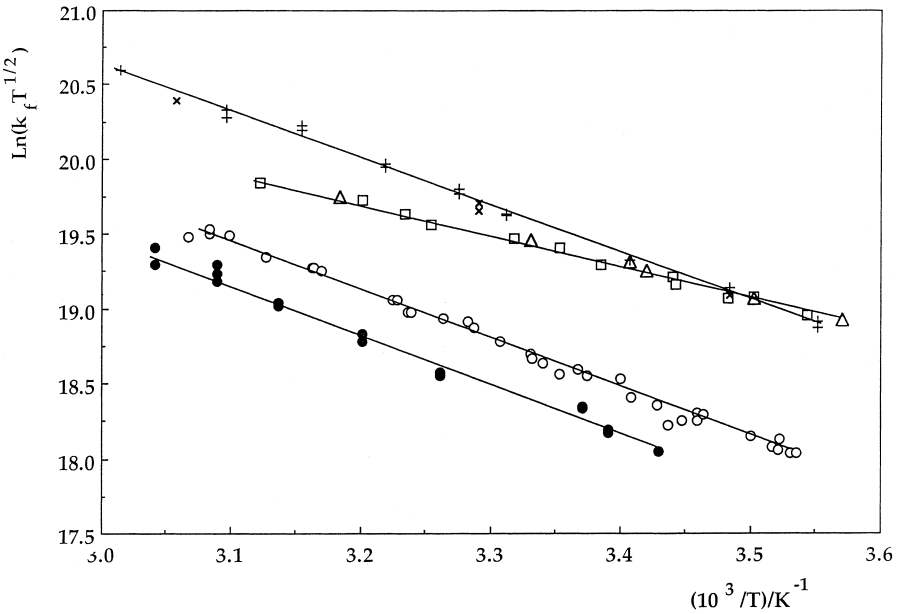

Fig. 2. Variation of ln ($k_{ET}T^{1/2}$) with reciprocal temperature in YE_4–porphyrin complex (○) at different concentrations in the range 30–200 μM; in WE_4–porphyrin complex at 90 μM (□) and 30 μM (△); in E_2YE_2 at 95 μM (×) and 30 μM (+); and in $YE_4G_{10}E$ at 90 μM (●). [$PdTMPyP^{4+}$] = 10 μM.

plotted according to Eq. (3) (Fig. 2). Analysis of the linear fits yielded values for the electron coupling matrix element H_{DA}, the reorganization energy λ and the activation energy E_a. The results are reported in Table 1. It is clear that H_{DA} values that were extracted from the intercept of plots such as those exemplified in Fig. 2 must be considered with caution. A small error on the intercept can induce a significant error in the value of H_{DA}. To minimize this, the variation of k_{ET} with temperature at different peptide concentrations was measured, thereby generating average values of H_{DA}. Measurements done with the YE_4–porphyrin complex (Fig. 2) yielded a relative error of approximately 15% on the electronic coupling matrix element, H_{DA}.

3.2. Molecular modeling

Molecular Dynamics (MD) simulations at 300 K were used to dock the peptide to the porphyrin without introducing human bias with regard to the geometry of the interaction. The porphyrin and peptide contacted each other approximately 3 ps after the start of these MD runs. For the next 22 ps, the mutual orientation of the two molecules continued to evolve and eventually reached a stable configuration at 300 K. Analysis of the MD docking trajectories showed, however, that the peptides folded rapidly into a limited set of conformations. Upon docking to the porphyrin, the pre-formed peptide conformation was invariably retained. This indicated that an adequate sampling of the energetically accessible peptide conformations complexed to porphyrin was not being obtained by the docking technique. The macroscopic sample comprises a thermodynamically averaged ensemble of energetically accessible conformations that must be simulated when modeling the average distance between the electron donor and acceptor groups. To obtain better sampling, the molecular dynamics technique Quenched Molecular Dynamics (QMD) [68,69] was employed. This has been shown to be an efficient way to sample the conformational space for a complex of this size [70].

The QMD technique makes use of high-temperature MD to overcome the energy barriers that separate conformations. Temperatures ranging between 600 and 1200 K were tested, and the Visual Molecular Dynamics (VMD) program [71] was employed to visually monitor the trajectories over the course of a given simulation. This showed that at lower temperatures (600–800 K) conformational energy barriers were not efficiently crossed, whereas at higher temperatures (> 1000 K) the complexes tended to dissociate. A reasonable compromise was found to be 1000 K. The MD visualizations showed that at 1000 K the peptides unfolded and refolded many times during 150 ps of QMD.

High-energy 'snapshots' obtained during the high temperature simulations were energy-minimized by MD cooling and reheated to 300 K for further sampling to obtain MD-averaged inter-chromophore distances. The root mean square deviations (RMSD) of the inter-chromophore distance did not exceed 30 pm during any given run, and in some cases were as low as 10 pm, showing fluctuations about a single stable configuration and attesting to the stability of the structures obtained from the QMD procedure. Conformational analysis showed that a variety of minimized structures were obtained for each complex with regard to the peptide conformation itself and/or the docking of the peptide to the porphyrin. Nevertheless, the total AMBER 5 energies calculated for different minimized structures for a given peptide–porphyrin complex were comparable. For example, for the YE_4 complexes the total energy averaged over 100 QMD minimized structures was -121 ± 7 kcal/mol. Furthermore, a plot of energy vs. inter-chromophore distances showed no correlation between these two parameters. The inter-chromophore distances calculated for the 50 structures obtained from each QMD run were averaged. For the YE_4 complex, the average of the distances obtained from the two QMD runs was essentially identical (810 ± 150 pm vs. 820 ± 140 pm), and therefore all 100 trajectories (50 from each QMD) were averaged to give the 816 ± 140 pm. The same reproducibility between runs was obtained for the WE_4 and E_2YE_2 complexes. Averaging over all 100 trajectories gave an average chromophore distance of 970 ± 160 pm and 800 ± 80 pm for the WE_4 and E_2YE_2 complexes,

respectively. The $YE_4G_{10}E$ complex, on the other hand, showed significant differences in the average distances obtained from the two QMD runs performed. The average inter-chromophore distances were calculated to be 950 ± 120 pm for the first set and 850 ± 120 pm for the second set, giving an average of 900 ± 130 pm over all trajectories measured. Being three times longer than the other peptides and containing 10 glycines, this peptide is considerably more flexible.

The mutual orientation of the chromophores was determined by averaging the angle between the porphyrin plane and the plane of the aromatic ring of the tyrosine or tryptophan over the same trajectories used to measure distances. All four complexes showed broad distributions for this angle with average values of approximately 48°. For the YE_4–complex, the average value was $47° \pm 19°$. Essentially the same average values were observed for the WE_4 ($48° \pm 17°$), E_2YE_2 ($48° \pm 17°$), and $YE_4G_{10}E$ complexes ($50° \pm 20°$).

The structures generated by QMD were analyzed with regard to the conformations of the peptides and their interactions with the porphyrin. In particular, the success of the QMD technique in sampling the conformational space of the peptide was assessed, as was the influence of the porphyrin on the conformations obtained. As discussed, once a particular conformation was equilibrated to 300 K, it changed very little, even after 200 ps of MD at that temperature. Therefore, one energy-minimized structure per trajectory (100 for each complex) was analyzed based on backbone conformation angles ϕ(C–N–CαC) and ψ(N–Cα–C–N) values and intra- and intermolecular electrostatic and H-bonding contacts.

Based on the torsional angle profile for each peptide, the conformations were grouped into related families. Although backbone conformations varied over a wide range, all complexes exhibited certain common structural characteristics. For example, the positively charged amino terminus was found to interact always with one or more carboxylate groups. These interactions usually included the terminal carboxyl group and one or more glutamate sidechains, depending on the conformation (usually the sidechains belonging to the fourth or fifth and, more rarely, the third residue). Many of the remaining carboxyl groups, as well as many of the carbonyl groups of the peptide, were found to interact directly with the porphyrin molecule. These intermolecular interactions determine the relative position of the peptide with respect to the porphyrin. In all structures, the pentapeptide was found on one side of the porphyrin plane. Both partially extended and folded conformations of the peptide were obtained. In most conformations, the peptide backbone folded back on itself, but did not appear to exhibit a classic beta-type turn as found in proteins, probably due to the influence of the porphyrin acting as a template. For example, the hydrogen bond observed in protein β-turns between the carbonyl oxygen of the first residue and the amide hydrogen of the fourth residue of the turn was not observed.

Examination of the backbone torsional angle profiles indicated that the YE_4 conformations could be placed in six major conformational families, designated as A through F. The distribution was as follows: A (41 structures); B (33 structures); C (4 structures); D (4 structures); E (6 structures); and F (12 structures). In Fig. 3 the upper panel compares the backbone torsional angles for representative structures from each family. The structures themselves are shown in the lower panel of Fig. 3 and are labeled A, B, C, D, E and F to correspond to the graph. One sees the variety of conformations and significant variation between these structures in the position of the electron-transfer active residues (Y) relative to the porphyrin. All these structures have comparable energies. The degree of variation within most families was quite small, as shown in Fig. 4 (corresponding to family E).

For the WE_4 complex, a similar variety of conformations was found, some partially extended and some folded. As for YE_4, all structures could be divided into six major conformational families: A (10 structures); B (26 structures); C (51 structures); D (2 structures); E (6 structures);and F (5 structures). The torsion-angle profile for these families is shown in Fig. 5 (upper panel). Representative structures for each family are depicted

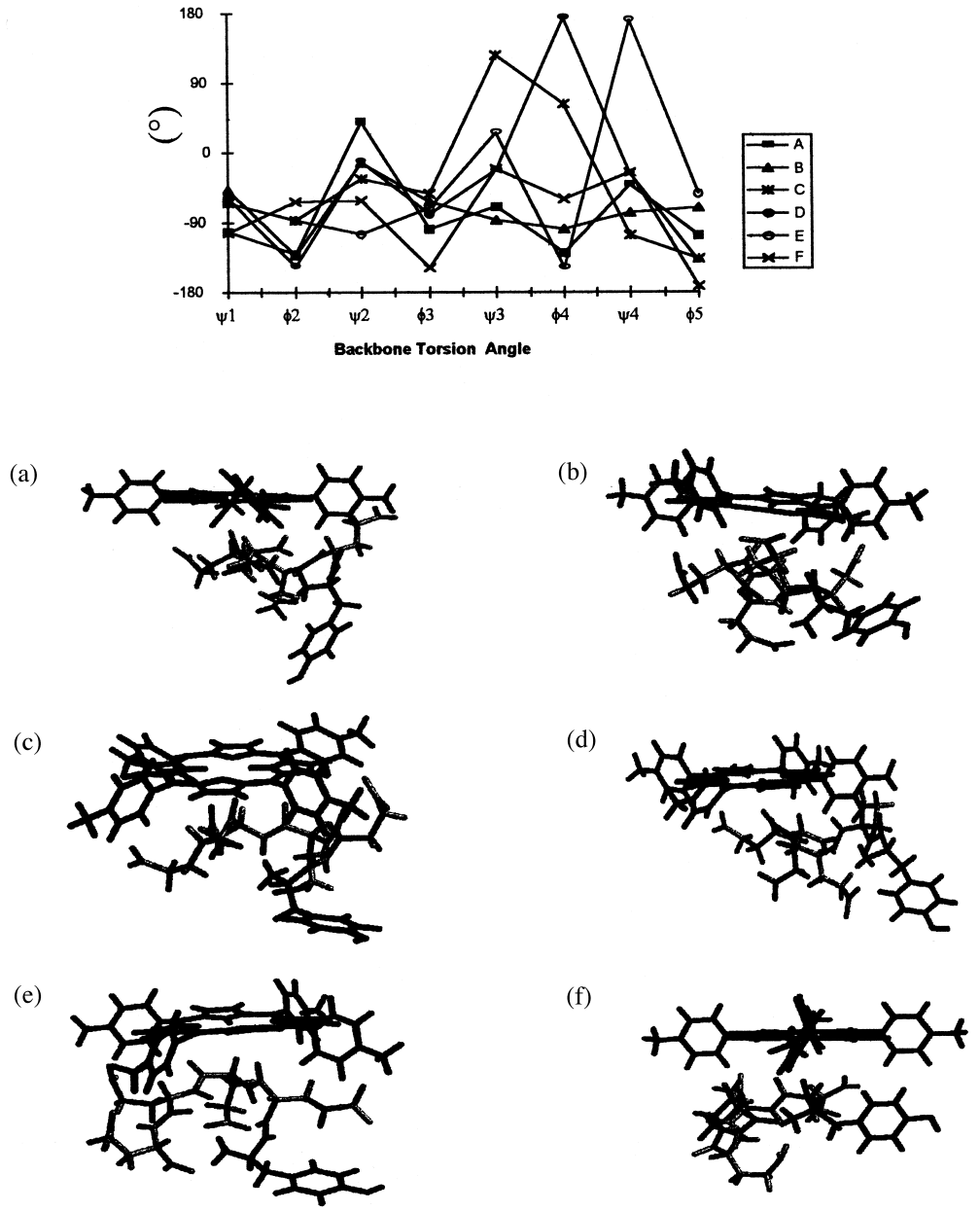

Fig. 3. Upper panel: backbone torsion angle profiles for representative structures from the six families of peptide conformations obtained for the YE_4–porphyrin complex by Quenched Molecular Dynamics. The peptide torsion angle ϕ_i and ψ_i are plotted from the *N*- to the *C*-terminus. Lower panel: Representative structures from each family.

on the lower panel of Fig. 5. One can see that conformational differences primarily occur at the $\psi 3$ and $\psi 5$ torsion angles.

For the E_2YE_2 pentapeptide, the analysis of torsion angles showed significantly less deviation. Four conformational families were identified for this complex: A (8 structures); B (15 structures); C (30 structures); and D (47 structures) (data not shown).

For the $YE_4G_{10}E$ peptide, the conformational

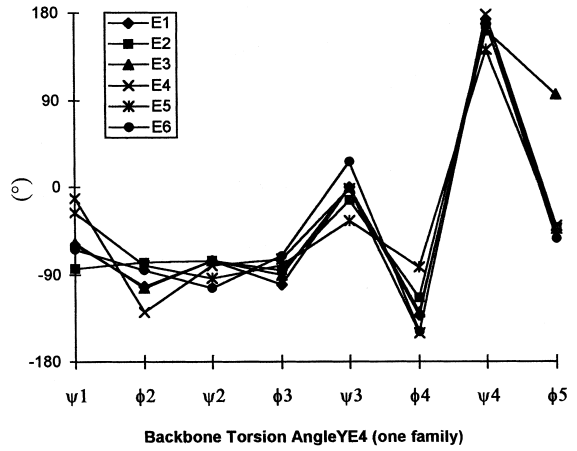

Fig. 4. Torsional angle profiles for the six YE_4 structures grouped as family E for the YE_4.

analysis did not yield discrete conformational families, as was anticipated from the numerous possible conformations of such a long peptide. However, the sidechains of the E residues in this peptide provided the same template for the porphyrin molecule as in the case of the other complexes. For this complex, QMD was not expected to give adequate sampling of the conformational space.

4. Discussion

4.1. Assumptions and justifications

Table 1 provides a summary of all the data, both kinetic and modeling, resulting from this study. However, prior to discussing the ramifications of these data, it is necessary to provide some explanations and justifications of the methods used and the assumptions made.

4.1.1. Molecular modeling

Molecular dynamics simulations of the peptide–porphyrin complexes were performed in order to ascertain whether such endeavors could be of use in understanding the kinetic data. For example, were the differences in the values of the matrix elements linking donor and acceptor (H_{DA}) connected with differences in inter-chromophore distance as determined from the MD simulations? This would be justified if inter-chromophore orientations were not significantly different for the systems compared. It was to be expected that the short peptides used in this study would be able to assume a variety of conformations and orientations when electrostatically associated with the porphyrin. Thus, any inter-chromophore distance arising from the calculations would be an average over a representative ensemble of structures. It became apparent in the preliminary docking experiments that room temperature MD did not adequately sample the conformational space of the peptide. This conclusion was drawn by observing that pre-folded peptides remained in essentially the same backbone conformation upon docking to the porphyrin. It was therefore, necessary to devise a method to more effectively sample the conformational space available to peptides when associated with the porphyrin. This led us to employ QMD. Moreover, local fluctuations of the Y and W sidechain chromophores observed during 300 K MD runs were large enough to make it equally apparent that it would not be sufficient to simply measure intra-chromophore distances in energy-minimized structures.

Based on the torsional angle profile for each peptide, the conformations were grouped into related families. A detailed analysis of one of the four porphyrin–peptide complexes (YE_4) was carried out to illustrate the conformational differences in the families identified. For YE_4 six major conformational families (A through F) were identified from backbone torsional angle profiles. Fig. 3 shows the backbone torsional angles and the structures of representative complexes from each family. This serves to illustrate the differences observed between conformations obtained, thus validating the effectiveness of QMD to generate different conformations of comparable energies. A question that could be raised regarding

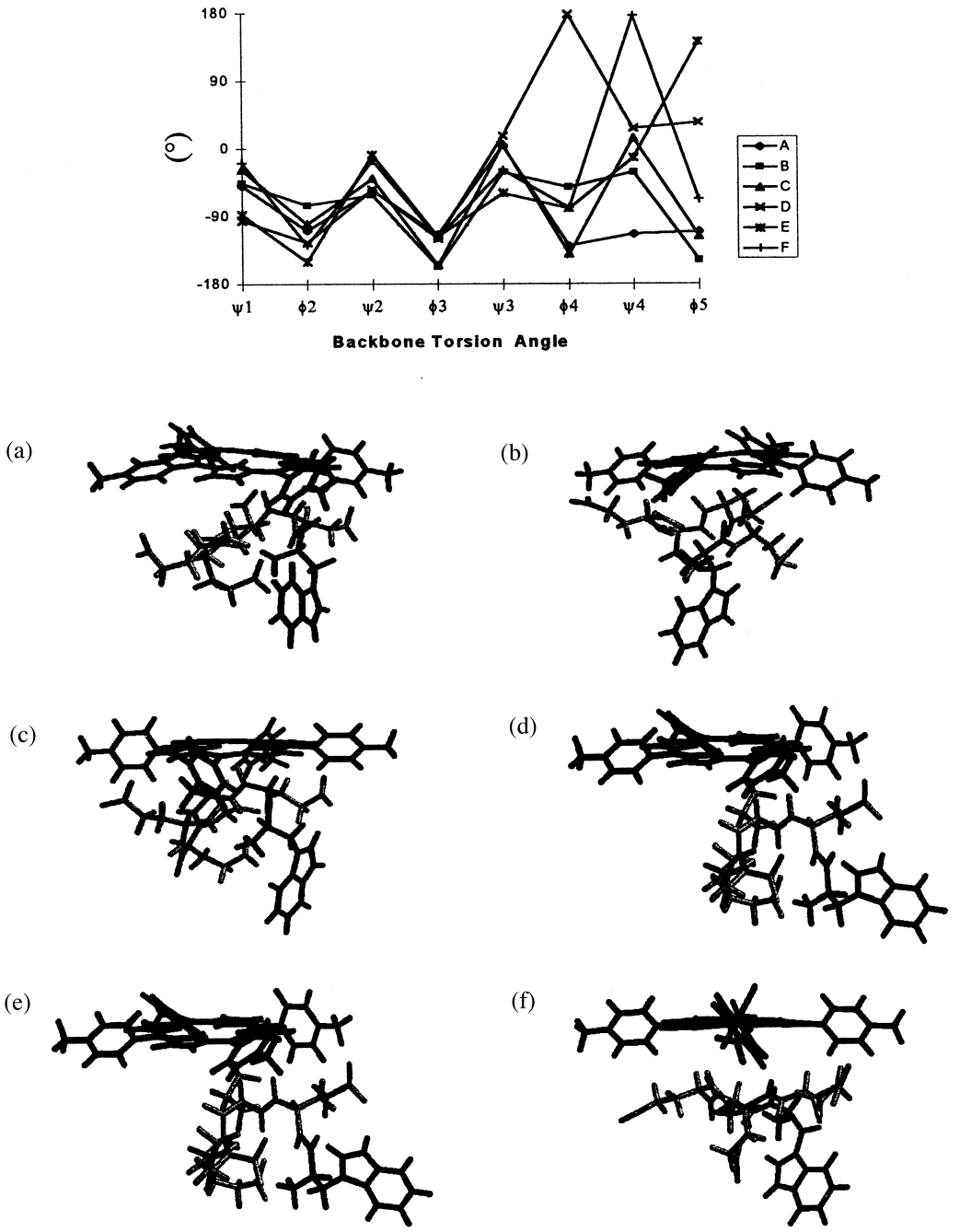

Fig. 5. Upper panel: backbone torsion angle profiles for representative structures from the six families of peptide conformations obtained for the WE_4–porphyrin complex by Quenched Molecular Dynamics. The peptide torsion angles ϕ_i and ψ_i are plotted from the *N*- to the *C*-terminus. Lower panel: representative structures from each family.

the sampling method is whether 100 structures adequately sample the conformational space for the purpose of calculating inter-chromophore distances. If every conformation obtained were different, the answer clearly would be in the negative. However, within most families the deviations in backbone angles were found to be relatively small. For example, the backbone profile for all the structures belonging to family E of complexes of type YE_4 are plotted in Fig. 4. Moreover, the average QMD distances obtained from separate sets of simulations (50 structures each) were essentially identical. These arguments lead to the conclusion that 100 samples are appropriate to provide good representations of the structures of the complexes; and even were 1000 samples to be undertaken, this would serve merely to increase the population within the families and to improve the precision on the data evaluated. By the same criteria, it was apparent that 100 structures did not adequately sample the much longer $YE_4G_{10}E$ peptide.

4.1.2. Temperature-dependent rate data

The solvent reorganization energies (λ) and electronic interaction energies (H_{DA}) shown in Table 1 were extracted from linear fits to Eq. (3). The data presented assume that both λ and ΔG^0 are independent of temperature over the range employed. However, fits to Eq. (3) may be 'linear' but still generate incorrect values for H_{DA} and λ. Thus, in a pulse radiolysis study of charge–shift reactions, Liang et al. [63] presented two plots of ln ($k_{ET}T^{1/2}$) vs. $1/T$. In one plot, the temperature dependence of λ and ΔG^0 were taken into account. In the other plot λ was fixed to the value at room temperature. Both plots were reasonably linear, but the different slopes and intercepts provided H_{DA} values (extracted from these intercepts) that differed by a factor of ~ 2.5. Thus, it is extremely important to show that fits to Eq. (3) (e.g. Fig. 2) are indeed generating the correct values for λ and H_{DA}.

The temperature dependence of λ is generally estimated based on a dielectric continuum model [13,14]:

$$\lambda = (e^2/4\pi\varepsilon_0)[1/2r_A + 1/2r_{DA}] \times [1/\varepsilon_{op} - 1/\varepsilon_s] \quad (4)$$

where ε_{op} and ε_s are the optical and static dielectric constants of the solvent, r_A and r_D are the radii of the spherical reactants and r_{DA} is the center-to-center donor/acceptor distance. With the not-unreasonable assumption that the ion-pair complex structure is independent of temperature within the range investigated (10–60°C), the dependence of λ over this temperature range can be estimated by the variation of the term $(1/\varepsilon_{op} - 1/\varepsilon_s)$. Using tabulated data for water [72], values of 0.5503 (at $T = 10$°C) and 0.5527 (at $T = 60$°C) were obtained for this dielectric constant term. Thus, over the range employed here, λ may be considered as practically temperature independent.

The free energy of reaction for charge separation, ΔG^0, can be estimated from the point-charge model [40]:

$$\Delta G^0 = (E_{ox} - E_{red}) - \Delta E_{00}^{T} - (4\pi\varepsilon_0)^{-1} e^2/r_{DA}\varepsilon_s \quad (5)$$

As for λ any temperature dependence of ΔG^0 will be concentrated in the dielectric constant term, ε_s. The charge separation distance, r_{DA}, the excitation energy, ΔE_{00}^{T}, of the S_0–T_1 0–0 transition, the oxidation potential, $E_{ox,}$ of the donor, and the ground state reduction potential of the acceptor, E_{red}, can be reasonably regarded as being independent of T. In fact, reduction potentials of $Pd(II)TMPyP^{4+}$ were measured over the temperature range 10–60°C and were found to be independent of T. Then putting $r_{DA} = 816$ pm (tyr–peptide), the Coulomb terms, $(4\pi\varepsilon_0)^{-1} e^2/r_{DA}\ \varepsilon_s$, were estimated to be 0.021 eV (at 10°C) and 0.022 eV (at 60°C), showing that ΔG^0 is only weakly dependent on the temperature over the range investigated. The same considerations hold for the trp–porphyrin complex. In the pulse radiolysis study reported by Liang et al. [63], a similar weak dependence of ΔG^0 with T was shown in the much larger temperature range from −94°C to 100°C. These considerations would appear to justify the assumptions that λ and ΔG^0

are independent of temperature and that the parameters presented in Table 1 for the intra-complex electron-transfer rate constant are indeed appropriate.

4.2. Data discussion

A prior report from this laboratory [53] stated that the intra-complex electron-transfer rate constant to the porphyrin triplet state from a pentapeptide where trp replaced tyr, namely, WE_4, was 1.4×10^7 s^{-1}, a factor of 2.1 times that for the YE_4 variant (6.6×10^6 s^{-1}). In the current study λ and H_{DA} values have been determined for these reactions, inter alia. Moreover, the ΔG^0 values at pH 7 for the oligopeptides are -0.18 eV (trp) and -0.25 eV (tyr). Thus Eq. (3) can be used to calculate the expected value of k_{trp}/k_{tyr} using the above parameters (derived from the temperature-dependence measurements of k_{ET}) and to compare this ratio to that computed from the experimentally determined room-temperature rate constants.

Eq. (3) leads to the following expression at fixed temperature:

$$k_{trp}/k_{tyr} = (\lambda_{trp}/\lambda_{tyr})^{-1/2}(H_{trp}/H_{tyr})^2 \times \exp(-\Delta F/4k_BT)$$

where

$$\Delta F = \left\{\left(\Delta G^0_{trp} + \lambda_{trp}\right)^2/\lambda_{trp}\right\} - \left\{\left(\Delta G^0_{tyr} + \lambda_{tyr}\right)^2/\lambda_{tyr}\right\} \quad (6)$$

Employing the data from Table 1 in Eq. (4), the λ term is 1.21, the H term is 0.046 and the exponential term is 34.1 when $k_BT = 25.7$ meV (at 298 K). The product of these terms is 1.90, only 10% lower than the experimental value of 2.1 for k_{trp}/k_{tyr} (i.e. within the uncertainty in the experimental determination of the intra-complex electron-transfer rate constant, which is approx. 10%). Thus, it is seen that the expression derived from Marcus' theory combined with experimental data from the temperature-dependence investigations allows a quantitative prediction of a quantity obtained from a completely independent set of experiments. For the tyrosine-only peptides, E_2YE_2 and YE_4, Eq. (6) is reduced to

$$k_{tyr}(E_2YE_2)/k_{tyr}(YE_4) = \left[H_{tyr}(E_2YE_2)/H_{tyr}(YE_4)\right]^2$$

From the experimental data (Table 1), the rate constant ratio is 2.22 and that of the H terms squared is 2.19 — again an excellent agreement. This internal consistency provides excellent support for the conclusion reached in the prior publication that the quenching of the porphyrin triplet states by the target amino acids resulted from an electron-transfer reaction [53].

Eq. (6) evaluates the ratio of any pair of rate constants through the application of the temperature-dependence measurements. This ratio can also be obtained from direct measurements of k_{ET} at room temperature (based on the observed quenching of the metalloporphyrin triplet state as shown in Fig. 1). This provides a useful diagnostic tool inasmuch as it allows an evaluation of whether the observed linear fit to Eq. (3) is indeed the appropriate one for yielding the correct values for λ and H_{DA}. Clearly, the excellent agreement found between these two different approaches is an indication that the linear fits to Eq. (3) are indeed yielding the correct values for λ and H_{DA}. Hence the assumptions that both λ and ΔG^0 are temperature independent over the range of temperature investigated are essentially correct for our systems.

As seen in Table 1, the intra-complex electron-transfer rate constants at 298 K were found to be similar for the two peptides with terminal Y residues, namely, $k_{ET} = 6.6\times10^6$ s^{-1} (YE_4) and $k_{ET} = 4.7\times10^6$ s^{-1} ($YE_4G_{10}E$). This is consistent with the experimental data derived from the temperature dependence that the electronic coupling matrix elements (H_{DA}) and reorganization energies λ were identical in these two tyr–peptide complexes. From this it is possible to infer that the donor–acceptor separation distance

and/or their relative orientation within the ion-pair complex as well as the polar environment of their surrounding medium are also similar.

Interestingly, in E_2YE_2 where the tyrosine residue is incorporated in the middle of the peptide backbone, the room-temperature rate constant was higher ($k_{ET} = 1.47 \times 10^7\ s^{-1}$) compared with those peptides where the tyrosine residue was attached at the end of the peptide chain. All the tyr-containing oligopeptides showed λ values of $\sim 1.60 \pm 0.05$ eV (Table 1), indicating that the oxidation of tyr and the reduction of porphyrin elicits an identical dipolar response of the surrounding medium. Thus, the higher electron-transfer rate constant measured for E_2YE_2 is probably a direct consequence of a stronger electronic coupling between tyrosine and the porphyrin triplet state as reflected by the derived value of $H_{DA} = 7.55$ meV (some 50% higher than the H_{DA} value when tyr is the terminal residue). This increased value of H_{DA} for the centrally located tyr is an indication that there is a higher degree of orbital overlap between the reacting partners (porphyrin T_1; tyr). However, molecular modeling indicated that the average distance between tyrosine and porphyrin is essentially similar in all the tyr–peptide complexes (Table 1). Thus, the higher coupling observed for E_2YE_2 may be a consequence of a more efficient orbital overlap due to more favorable ring–ring orientation.

Another interesting observation is that in all three tyr–peptide complexes at neutral pH, values of λ were large ($\sim 1.6 \pm 0.05$ eV). This can be taken to indicate a relatively high medium polarity surrounding the tyrosine residue, irrespective of whether tyrosine is attached to the end of the peptide chain or incorporated in the middle. Therefore, in these complexes tyrosine residues are probably exposed to the aqueous medium in a similar way. The independent measurement of the reduction potentials strongly supports this conclusion, as it was found that the E^0 values of tyrosine and tryptophan residues incorporated within the peptide matrix were identical to the reduction potential of monomeric tyrosine and tryptophan in water.

As shown in Table 1, reorganization energies λ measured for YE_4 and WE_4 are significantly different. The value of $\lambda = 1.08$ eV for E_4W is within the range of reorganization energies measured for other electron-transfer systems, viz., 0.7–1.3 eV [73]. The value of $\lambda = 1.57$ eV derived for E_4Y is significantly larger. The solvent contribution to the reorganization energy increases with solvent polarity [63], and the observed difference in tyr–peptide and trp–peptide may reflect a more hydrophilic environment around the phenolic group of tyr residue compared to that of the terminal indole group of trp residue. This is consistent with the expected strong hydrogen bonding between solvent molecules and the tyrosine hydroxyl group. The reported hydrophobicity scale for amino acids based on partition of residues between protein surface and interior [74] also supports such hydrophilicity considerations. On this scale, the measured transfer free energies surface/interior ($\Delta G^0_{tr,s/i}$) were -0.22 kcal mol^{-1} and $+0.44$ kcal mol^{-1} for tyrosine and tryptophan, respectively, confirming again a considerably higher hydrophilicity for tyrosine relative to that for tryptophan residue. It should also be noted that other large values for reorganization energies were reported. Thus, $\lambda = 1.9$ eV has been measured for electron transfer between methanol dehydrogenase and cytochrome *c*-551i [75] and $\lambda = 2.3$ eV for electron transfer between methylamine dehydrogenase and amicyanin [76]. These large values were attributed to conformational changes and/or configurational realignment after complex formation for optimal electron transfer. Values in the range 2.0–2.3 eV were also estimated for photoinduced electron transfer with binuclear complexes of Ru(II)–Co(III) in butyronitrile [77].

Significantly different values of H_{DA} were also derived for YE_4 (5.1 meV) and WE_4 (1.1 meV) from the temperature-dependence plots, reflecting a stronger electronic coupling between the tyrosine residue and the porphyrin triplet state as compared to that in the trp–peptide complex. Electronic coupling depends on the type of interactions between the donor and acceptor. Thus, the higher value of H_{DA} for tyrosine-containing pentapeptide (YE_4) supports the assumptions that (a) tyrosine residues are, on average, closer to

porphyrin than tryptophan residues; and/or (b) a more efficient orbital overlap exists between tyrosine and porphyrin compared to that between tryptophan and porphyrin. In this case, in both systems YE_4-PdTMPyP^{4+} and WE_4-PdTMPyP^{4+}, the electronic coupling matrix element H_{DA} will be essentially responsible for the dependence of the rate constant k_{ET} on the donor–acceptor separation distance and/or their relative orientation. As will be seen below, such a conclusion is in agreement with results derived from molecular modeling studies.

In the earlier publication from this laboratory it was demonstrated that the quenching of the porphyrin T_1 state by either trp or tyr involves an electron-transfer event [53]. This was inferred from a study of the effect of pH-induced alteration of the intra-complex rate component and from the use of metalloporphyrins having different reduction potentials. The present work provides additional data to support the contention that electron transfer is indeed the rate-determining factor at pH 7.0 via measurements of the reorganization energy (λ) at different pH values. Thus, temperature dependence measurements of k_{ET} were conducted at pH 8.2 for YE_4. Analysis of the linear variation of ln ($k_{ET}T^{1/2}$) vs. $1/T$ yielded $\lambda = 1.65$ eV and $H_{DA} = 5.3$ meV, values similar to those determined at neutral pH. This is consistent with the proposal that although there might be an eventual proton transfer between oxidized tyr radicals and solvent molecule, this is not the rate-determining factor.[1] However, this proton transfer may explain the relatively high reorganization energy ($\lambda \sim 1.6$ eV) observed for the tyrosine–peptide complex. It is recalled that the total reorganization energy $\lambda = \lambda_s + \lambda_{in}$, where λ_s is the solvent contribution and λ_{in} is the energy necessary for reorganization of the nuclear frameworks of the reacting and product species. Thus, a proton transfer process occurring prior to the electron-transfer event may induce a change on the nuclear configuration of the redox partners, which in turn may provoke a relatively high nuclear reorganization energy for the electron-transfer reaction. Molecular modeling considerations are in agreement with the experimentally determined electronic coupling matrix elements H_{DA}, strongly suggesting that electronic coupling between the redox partners is primarily responsible for the dependence of the electron-transfer rate constant on the donor–acceptor separation distance and their relative orientation. Thus, from the models shown in Figs. 3 and 5 and the results displayed in Table 1, stronger coupling would be expected in the YE_4/porphyrin complex than in the WE_4/porphyrin complex owing to the relatively shorter average distance between redox partners.

It is also worth noting that the use of Eq. (3) to determine the electronic coupling matrix element H_{DA} is based on the assumption that the electron-transfer reaction is non-adiabatic. The division between adiabatic or non-adiabatic varies with the system but, as a general rule [78], the point of demarcation is usually placed at $H_{DA} =$ 25 mV (namely kT at 300 K). The magnitude of the two electronic coupling matrix elements derived in tyr–peptide (~ 5.1 mV) and trp–peptide (1.1 mV) are clearly typical of a relatively weak non-adiabatic electron-transfer reaction, i.e. in accord with the assumption previously made.

Non-adiabatic electron transfer has also been described by a quantum-mechanical theory [78]. In this approach, the rate constant still derives from the Fermi Golden rule expression [(Eq. (1))] where now H_{DA} is the quantum mechanical counterpart of the classical electronic coupling matrix element, which also displays an exponential dependence with distance:

$$H_{DA}(\mathrm{cm}^{-1}) = 10^5 \; e^{-\beta r} \qquad (7)$$

where r is the actual separation distance between donor and acceptor within the encounter complex and β is a measure of the ability of an orbital to extend into space and interact with another orbital. Since H_{DA} was determined experimentally,

[1] In fact, the effect of pH was reflected by a red shift of PdTMPyP^{4+} Soret band, with a lessening of the absorption intensity at the band maximum. Interestingly, this behavior parallels [53] that observed with the effect of peptide concentration on the ground state absorption of PdTMPyP^{4+}. Thus, the effect of pH is simply reflecting evidence for ion association that increases with pH.

Eq. (7) can be employed to estimate β Clearly, such a procedure requires knowledge of r, and complications can arise in the identification of this distance, especially in large redox systems such as those employed here. In the determination herein, the distance between donor and acceptor is taken as the average distance between the center of mass (COM) of the porphyrin ring and the COM of the tyrosine or tryptophan target. These distances were derived from the molecular modeling calculations. The overlap parameter (β) values are listed in Table 1. Interestingly, values determined for YE_4, E_2YE_2 and WE_4 are similar (~ 0.9 Å^{-1}). A rather lower β value (0.85 Å^{-1}) was derived for the $YE_4G_{10}E$/porphyrin complex. As mentioned earlier, QMD is not expected to give good sampling for this much-longer peptide, and the value of r for this peptide/porphyrin complex may have been overestimated.

The tunneling pathway parameters (β) in Table 1 were obtained from Eq. (7) using separation distances between donor (Y and W residues) and acceptor (porphyrin triplet) within the association complex. These distances resulted from molecular modeling calculations as the average distance between the center of mass (COM) of the porphyrin ring and that of the aromatic residue ring. The question might be raised as to whether such distances have any real meaning. To examine this, it is recalled that Moser and Dutton have defined the critical distance for electron transfer as that from the edge of the donor to the edge of the acceptor [79]. They proposed an empirical rate expression (based on an extensive review of data on native intra-protein electron transfer at room temperature) of the following form:

$$\log k_{ET} = 15 - 0.6r - 3.1(\Delta G^0 + \lambda)^2/\lambda \qquad (8)$$

where r (Å) is defined as the edge-to-edge distance between donor and acceptor pair, ΔG^0 (eV) is the free energy and λ(eV) is the reorganization energy. This relation was shown to be relatively successful as a first approximation for various electron-transfer rates in photosynthetic reaction centers [79], the standard deviation between the predictions of Eq. (8) and measurements of native intra-protein electron-transfer rates being approximately 0.4 log units or a factor of 2.4. In the present work the values of k_{ET}, ΔG^0 and λ have been determined experimentally, thereby allowing a test to be made of the applicability of Eq. (8) for the oligopeptides used here. Thus the data in Table 1 lead to values of $r = 790$ pm for YE_4, $r = 794$ pm for $YE_4G_{10}Y$, $r = 737$ pm for E_2YE_2, and $r = 921$ pm for WE_4. These are listed in Table 1 for comparison with the molecular modeling results. Clearly, the values obtained from the Moser–Dutton relationship agree well with those obtained by the molecular modeling, with the possible exception of the long peptide $YE_4G_{10}E$, for which the QMD sampling technique was inadequate. However, the sidechains of the E residues in this peptide still provided the same template for the porphyrin molecule as in the case of the other complexes. Also, the observation that the experimentally derived H_{DA} parameters for YE_4 and $YE_4G_{10}E$ are identical may indicate a similar donor–acceptor separation distance in these two complexes as found from derivation based on the Moser–Dutton equation (Table 1). Furthermore, it can be seen that employing a value of $r = 794$ pm (derived from the Moser–Dutton equation) for the $YE_4G_{10}E$ complex in Eq. (7) yields a value of $\beta = 0.97$ Å^{-1}, i.e. similar to β values determined for the other complexes.

5. Concluding remarks

The association between the anionic oligopeptides and the cationic porphyrins leading to self-assembled electrostatically bound ion-pair complexes has been demonstrated to be useful for bringing the electron-transfer donor and acceptor into spatial proximity. The hypothesis stated and tested in the previous publication in this series [53] was that the porphyrin's rigid π-system provided a tetracationic template at which four CO_2^- functionalities (provided by glutamic acid residues) could be associated. This hypothesis was derived largely from chemical intuition. The kinetic data obtained in this work and the earlier one [53] support the concept, but a quantitative

study clearly requires knowledge of the structure of the complex prior to the light-absorption event. However, NMR investigations were inconclusive. ^{1}H-NMR spectra show that all the glutamate resonances largely overlap each other. This could be anticipated from the modeling studies that demonstrated that the peptides bind in a variety of conformations which are in dynamic equilibrium on time scales shorter that those required for NMR structural determination. These conformations share certain general features (such as position of the carboxylates close to the pyridinium groups), but the overall flexibility in the bound peptide will lead to broadened or averaged resonances due to the exchange (on the relevant NMR time scales — microseconds to milliseconds) between different states of the system.

Meanwhile, the molecular dynamics simulations reported here have helped to support the hypothesis. The Quenched Molecular Dynamics procedure generated a variety of structures that could be grouped into a limited number of conformational families. This allows the conclusion that the conformational space for the three pentapeptides (WE_4, YE_4, and E_2YE_2) bound to porphyrin was being adequately sampled. The calculated average COM distances, porphyrin-to-trp/tyr, were reasonable, as indicated by the application of the Moser–Dutton relationship using the kinetic parameters arrived at from the temperature-dependent rate constant study. This agreement lends a degree of confirmation to the usefulness of such modeling to obtain donor–acceptor distances in complexes held together solely by electrostatic forces.

Acknowledgements

This work was supported in part by NIH grants 2RO1-CA46281 (to MAJR) and 1R15-GM55898 (to NBL) and by the Center for Photochemical Sciences at Bowling Green State University.

References

[1] G.A. Mines, M.J. Bjerrum, M.G. Hill et al., Rates of heme oxidation and reduction in Ru(His33)cytochrome *c* at very high driving forces, J. Am. Chem. Soc. 118 (1996) 1961–1965.

[2] J.R. Scott, A. Willie, M. McLean et al., Intramolecular electron transfer in cytochrome b_5 labeled with ruthenium(II) polypyridine complexes: Rate measurements in the Marcus inverted region, J. Am. Chem. Soc. 115 (1993) 6820–6824.

[3] J.S. Zhou, S.T. Tran, G. McLendon, B.M. Hoffman, Photoinduced electron transfer between cytochrome *c* peroxidase (D37K) and Zn-substituted cytochrome *c*: probing the two-domain binding and reactivity of the peroxidase, J. Am. Chem. Soc. 119 (1997) 269–277.

[4] K. Wang, H. Mei, L. Geren et al., Design of a ruthenium–cytochrome *c* derivative to measure electron transfer to the radical cation and oxyferryl heme in cytochrome *c* peroxidase, Biochemistry 35 (1996) 15107–15119.

[5] A. Willie, M. McLean, R-Q. Liu et al., Intracomplex electron transfer between ruthenium-65-cytochrome b_5 and position-82 variants of yeast iso-1-cytochrome *c*, Biochemistry 32 (1993) 7519–7525.

[6] D.N. Beratan, J.N. Onuchic, H.B. Gray, Metal Ions in Biological Systems, in: H. Sigel, A. Sigel (Eds.), Electron Tunneling Pathways in Proteins, 27, Marcel Dekker, New York, 1991, p. 97.

[7] R.A. Marcus, The theory of oxidation–reduction reactions involving electron transfer, J. Chem. Phys. 24 (1956) 966–978.

[8] J. Jortner, M. Bixon, Intramolecular vibrational excitations accompanying solvent-controlled electron transfer reactions, in: R. Austin, E. Buhks, B. Chance, D. DeVault, P.L. Dutton, H. Frauenfelder, V.I. Gol'danskii (Eds.), Protein Structure: Molecular and Electronic Reactivity, Springer-Verlag, New York, 1987, p. 277.

[9] M. Bixon, J. Jortner, M.E. Michel-Beyerle, A. Ogrodnik, A superexchange mechanism for the primary charge separation in photosynthetic reaction centers, Biochim. Biophys. Acta. 977 (1989) 273–286.

[10] R.A. Marcus, N. Sutin, Electron transfer in chemistry and biology, Biochim. Biophys. Acta. 811 (1985) 265–322.

[11] J.R. Miller, J.V. Beitz, R.K. Huddleston, Effect of free energy on rates of electron transfer between molecules, J. Am. Chem. Soc. 106 (1984) 5057–5068.

[12] I.R. Gould, D. Ege, S.L. Mattes, S. Farid, Return electron transfer within germinate radical ion pairs. Observation of the Marcus inverted region, J. Am. Chem. Soc. 109 (1987) 3794–3796.

[13] T. Ohno, A. Yoshimura, N. Mataga, Bell-Shaped energy-gap dependence of backward electron transfer occuring within geminate radical pairs produced by quenching of ruthenium(II) polypyridine complexes by aromatic amines, J. Phys. Chem. 94 (1990) 4671–4876.

[14] J.C. Facelli, M. Barfield, Importance of multicenter integrals in semiempirical calculations of nuclear spin–spin coupling constants. 1. Isotropic coupling, J. Am. Chem. Soc. 106 (1984) 3407–3413.

[15] M.R. Wasielewski, M.P. Niemczyk, W.A. Svec, E.B. Pe-

witt, Dependence of rate for photoinduced charge separation and dark charge recombination on the free energy of reaction in restricted-distance porphyrin–quinone molecules, J. Am. Chem. Soc. 107 (1985) 1080–1082.

[16] R.A. Marcus, Theory of electrochemical and chemical electron transfer processes, Can. J. Chem. 39 (1959) 155–163.

[17] G. Grampp, G. Rauhut, Experimental and theoretical estimations of the solvent independence of the electronic coupling matrix element for an organic homogeneous electron self-exchange reaction, J. Phys. Chem. 99 (1995) 1815–1818.

[18] P. Finckh, H. Heitele, M. Volk, M.E. Michel–Beyerle, Electron donor/acceptor interaction and reorganization parameters from temperature-dependent intermolecular electron-transfer rates, J. Phys. Chem. 92 (1988) 6584–6590.

[19] P. Siddarth, R.A. Marcus, Electron-transfer reactions in proteins: electronic coupling in myoglobin, J. Phys. Chem. 97 (1993) 6111–6114.

[20] P. Siddarth, R.A. Marcus, Calculation of electron-transfer matrix elements of bridged systems using a molecular fragment approach, J. Phys. Chem. 96 (1992) 3213–3217.

[21] P. Siddarth, R.A. Marcus, Electron-transfer reactions in proteins: a calculation of electronic coupling, J. Phys. Chem. 94 (1990) 8430–8434.

[22] J.J. Regan, S.M. Risser, D.N. Beratan, J.N. Onuchic, Protein electron transport: single versus multiple pathways, J. Phys. Chem. 97 (1993) 13083–13088.

[23] D.N. Beratan, J. Betts, J.N. Onuchic, Protein electron transfer rates set by the bridging secondary and tertiary structures, Science 252 (1991) 1285–1288.

[24] J.N. Betts, D.N. Beratan, J.N. Onuchic, Mapping electron tunneling pathways: an algorithm that finds the 'minimum length'/maximum coupling pathway between electron donors and acceptors in proteins, J. Am. Chem. Soc. 114 (1992) 4043–4046.

[25] M.S. Workentin, F. Maran, D.D.M. Wayner, Reduction of di-tert-butyl peroxide: evidence for nonadiabatic dissociative transfer, J. Am. Chem. Soc. 117 (1995) 2120–2121.

[26] J-M. Savéant, A simple model for the kinetics of dissociative electron transfer in polar solvents, J. Am. Chem. Soc. 109 (1987) 6788–6795.

[27] J-M. Savéant, Dissociative electron transfer. New tests of the theory in the electrochemical and homogeneous reduction of alkyl halides, J. Am. Chem. Soc. 114 (1992) 10595–10602.

[28] C.P. Andrieux, A. Le Gorande, J-M. Savéant, Electron transfer and bond breaking. Examples of passage from a sequential to a concerted mechanism in the electrochemical reductive cleavage of arylmethyl halides, J. Am. Chem. Soc. 114 (1992) 6892–6904.

[29] Y-P. Liu, M.D. Newton, Reorganization energy for electron transfer at film-modified electrode surfaces: a dielectric continiuum model, J. Phys. Chem. 98 (1994) 7162–7169.

[30] B.S. Brunschwing, S. Ehrenson, N. Sutin, Solvent reorganization in optical and thermal electron-transfer processes, J. Phys. Chem. 90 (1986) 3657–3668.

[31] B.S. Brunschwing, S. Ehrenson, N. Sutin, Solvent reorganization in optical and thermal electron-transfer processes: solvatochromism and intramolecular electron-transfer barriers in spheroidal molecules, J. Phys. Chem. 91 (1987) 4714–4723.

[32] Y-P. Liu, M.D. Newton, Solvent reorganization and donor/acceptor coupling in electron-transfer processes: self-consistent reaction field theory and ab initio applications, J. Phys. Chem. 99 (1995) 12382–12386.

[33] K. Ohta, G.L. Closs, K. Morokuma, N.J. Green, Stereoelectronic effects in intramolecular long-distance electron transfer in radical anions as predicted by ab initio MO calculations, J. Am. Chem. Soc. 108 (1986) 1319–1320.

[34] J.M. Gruschus, A. Kuki, New Hamiltonian model for long-range electronic superexchange in complex molecular structures, J. Phys. Chem. 97 (1993) 5581–5593.

[35] J.N. Onuchic, A predictive theoretical model for electron tunneling pathways in proteins, J. Phys. Chem. 92 (1990) 722–7733.

[36] P. Siddarth, R.A. Marcus, Electron-Transfer reactions in proteins: an artificial intelligence approach to electronic coupling, J. Phys. Chem. 97 (1993) 2400–2405.

[37] C.C. Moser, J.M. Keske, K. Warncke, R.S. Farid, P.L. Dutton, Nature of biological electron transfer, Nature 355 (1992) 796–802.

[38] G.L. Closs, L.T. Calcaterra, N.G. Green, K.W. Penfield, J.R. Miller, Distance, stereoelectronic effects, and the Marcus inverted region in intramolecular electron transfer in organic radical ions, J. Phys. Chem. 90 (1986) 3637–3683.

[39] J.W. Evenson, M. Karplus, Effective coupling in bridged electron transfer molecules: computational formulation and examples, J. Chem. Phys. 96 (1992) 5272–5278.

[40] G.C. Walker, E. Akesson, A.E. Johnson, N.E. Levinger, P.F. Barbara, Interplay of solvent motion and vibrational excitation in electron-transfer kinetics: experiment and theory, Phys. Chem. 96 (1992) 3728–3736.

[41] P.F. Barbara, G.C. Walker, T.P. Smith, Vibrational modes and the dynamic solvent effect in electron and proton transfer, Science 256 (1992) 975–981.

[42] J.D. Simon, S. Su, Intramolecular electron transfer and solvation, J. Chem. Phys. 87 (1987) 7016–7023.

[43] J.D. Cortes, H. Heitele, J. Jortner, Band-shape analysis of the charge-transfer fluorescence in barrelene-based electron donor-acceptor compounds, J. Phys. Chem. 98 (1994) 2527–2536.

[44] T. Asahi, M. Ohkohchi, R. Matsusaka et al., Intramolec-

ular photoinduced charge separation and charge recombination of the product ion pair states of a series of fixed-distance dyads of porphyrins and quinones: energy gap and temperature dependences of the rate constants, J. Am. Chem. Soc. 115 (1993) 5665–5674.

[45] A. Hormann, W. Jarzerba, P.F. Barbara, Ultrafast relaxation and electron transfer in optically prepared 'simple' ions pairs, J. Phys. Chem. 99 (1995) 2006–2015.

[46] K.W. Penfield, J.R. Miller, M.N. Paddon-Row, E. Cotsaris, A.M. Oliver, N.S. Hush, Optical and thermal electron in rigid di-functional molecules of fixed distance and orientation, J. Am. Chem. Soc. 109 (1987) 5061–5965.

[47] M. Woodle, J.W. Zhang, D. Mauzerall, Kinetics of charge transfer at the lipid bilayer–water interface on the nanosecond time scale, Biophysical journal 52 (1987) 577–586.

[48] J.S. Zhou, E.S.V. Granada, N.B. Leontis, M.A.J. Rodgers, Photoinduced electron transfer in self-associated complexes of several uroporphyrins and cytochrome *c*, J. Am. Chem. Soc. 112 (1990) 5074–5078.

[49] J.S. Zhou, M.A.J. Rodgers, Driving force dependence of rate constants of electron transfer within cytochrome *c* and uroporphyrin complexes, J. Am. Chem. Soc. 113 (1991) 7728–7734.

[50] C. Turro, C.K. Chang, G.E. Leroi, R.I. Cukier, D.G. Nocera, Photoinduced electron transfer mediated by a hydrogen-bonded interface, J. Am. Chem. Soc. 114 (1992) 4013–4015.

[51] J.L. Sessler, B. Wang, A. Harriman, Long-range photoinduced electron transfer in an associated but noncovalently linked photosynthetic model system, J. Am. Chem. Soc. 115 (1993) 10418–10419.

[52] K. Weidemaier, H.L. Tavernier, S.F. Swallen, M.D. Fayer, Photoinduced electron transfer and geminate recombination in liquids, J. Phys. Chem. A 101 (1997) 1887–1902.

[53] M. Aoudia, M.A.J. Rodgers, Photoprocesses in self-assembled complexes of oligopeptides with metalloporphyrins, J. Am. Chem. Soc. 119 (1997) 12859–12868.

[54] N.R. Kestner, J. Logan, J. Jortner, Thermal electron transfer reactions in polar solvents, J. Phys. Chem. 78 (1974) 2148–2166.

[55] P. Siders, R.A. Marcus, Quantum effects in electron transfer reactions, J. Am. Chem. Soc. 103 (1981) 741–747.

[56] M. Bixon, J. Jortner, Quantum effects on electron transfer processes, Faraday Discuss. Chem. Soc. 74 (1982) 17–29.

[57] J.R. Bolton, M.D. Archer, in: Basic electron-transfer theory, advances in chemistry series, In: J.R. Bolton, N. Mataga, G. McLendon (Eds.), Basic Electron-Transfer Theory, American Chemical Society, Washington, DC, 1991, pp 7.

[58] R.A. Marcus, Electron, proton and related transfers, J. Faraday Discuss. Chem. Soc. 74 (1982) 7–15.

[59] N. S. Hush, Homogeneous and heterogeneous optical and thermal electron transfer, Electrochim. Acta. 13 (1968) 1005–1023.

[60] N. Sutin, Theory of electron transfer reaction: insights and hindsights, Prog. Inorg. Chem. 30 (1983) 4411–4498.

[61] P. Finckh, H. Heitele, M. Volk, M.E. Michel-Beyerle, Electron donor/acceptor interaction and reorganization parameters from temperature-dependent intramolecular electron transfer rates, J. Phys. Chem. 92 (1988) 6584–6590.

[62] Y. Zeng, M.B. Zimmt, Symmetry effects on electron-transfer reactions: temperature dependence as a diagnostic tool, J. Phys. Chem. 96 (1992) 8395–8403.

[63] N. Liang, J.R. Miller, G.L. Closs, Correlating temperature dependence to free energy dependence of intramolecular long-range electron transfers, J. Am. Chem. Soc. 111 (1989) 8740–8741.

[64] B.D. Rihter, M.E. Kenney, W.E. Ford, M.A.J. Rodgers, Photochromic reactions involving palladium(II) octabutoxynaphtalocyanine and molecular oxygen, J. Am. Chem. Soc. 115 (1993) 8146–8152.

[65] K.G. Kevin, L.H. Pearl, S. Neidle, Molecular modeling of the interactions of tetra-(4-*N*-methylpyridyl) porphin with TA and CG sites on DNA, Nucleic Acids Res. 15 (1987) 6553–6562.

[66] D.A. Case, D.A. Pearlman, J.W. Caldwell et al. AMBER 5, University of California, San Francisco, 1997.

[67] W.D. Cornell, P. Ciepalk, C.I. Bayly et al., A second generation force field for the simulation of proteins, nucleic acids, and organic molecules, J. Am. Chem. Soc. 117 (1995) 5179–5197.

[68] R. Elber, M. Karplus, Multiple conformational states of proteins: a molecular dynamics analysis of myoglobin, Science 235 (1987) 318–321.

[69] F.H. Stillinger, T.A. Weber, Hidden structures in liquids, Phys. Rev. A 25 (1982) 978–989.

[70] G.V. Nikiforovich, Computational molecular modeling in peptide design, Int. J. Pept. Protein Res. 44 (1994) 513–531.

[71] F.W. Humphrey, A. Dalke, K. Shulten, VMD — visual molecular dynamics, J. Mol. Graphics. 14 (1996) 33–38.

[72] J.A. Dean, (Eds.), Lange's Handbook of Chemistry, 13th Ed., McGraw-Hill, New York, 1985.

[73] M.J. Thieren, M.A. Selman, H.B. Gray, I.J. Chang, J.R. Winkler, Long-Range electron transfer in ruthenium-modified cytochrome *c*: evaluation of porphyrin–ruthenium electronic couplings in the *candida krusei* and horse heart proteins, J. Am. Chem. Soc. 112 (1990) 2420–2422.

[74] S. Miller, J. Janin, A.M. Lesk, C. Clothia, Interior and surface of monomeric proteins, Mol. Biol. 196 (1987) 641–656.

[75] T.K. Harris, V.L. Davidson, Binding and electron transfer reactions between methanol dehydrogenase and its

physiologic electron acceptor cytochrome *c*-551I: a kinetic and thermodynamic analysis, Biochemistry 32 (1993) 14145–14150.

[76] H.B. Brooks, V.L. Davidson, Kinetic and thermodynamic analysis of a physiologic intermolecular electron-transfer reaction between methylamine dehydrogenase and amicyanin, Biochemistry 33 (1994) 5696–5701.

[77] A. Yoshimura, K. Nozaki, N. Ikeda, T. Ohno, Photoinduced electron transfer and back electron transfer reaction within binuclear complexes of Ru(II) and Co(III), J. Am. Chem. Soc. 115 (1993) 7521–7522.

[78] G.J. Kavarnos, Fundamental of Photoinduced Electron Transfer, VCH Publishers Inc, New York, 1993.

[79] C.C. Moser, P.L. Dutton, Engineering protein structure for electron transfer function in photosynthesis reaction centers, Biochim. Biophys. Acta. 1101 (1992) 171–1176.